

Temperature effect on structural and optical properties of V₂O₅ thin films prepared by spray pyrolysis technique

Asmaa Mrigal^{1*}, Lahocine El Gana¹, Mouhamed Addou^{1,2}, Khadija Bahedi³, Rajae Temsamani², Hajar Cherrad¹, Zouhir El Jouad^{1,2}, and Jamal Zimou¹

¹ Laboratory Optoelectronics and Physical Chemistry of Materiaux. Ibn Tofail University, Kenitra, Morocco.

² Laboratory of Materials and Valuation of the Resources of the Sciences and Techniques. AbdelmalekEssaadi University, B.P.416 – Tangier – Morocco.

³ Materials and Renewable Energies Laboratory. IbnZohrUniversity, Faculty of Sciences BP 8106 - Dakhla- Agadir-Morocco.

Abstract. In this work, the effect of substrate temperature on structural and optical properties of V₂O₅ thin films has been characterized by X-ray diffraction (XRD); SEM and transmission. The films mince has been prepared by Reactive Chemical Spraying technology in Liquid Phase (RCSLP) on glass substrates preheated at (350, 400, 450 and 500 °C). The X-ray diffraction analysis confirms that all layers are polycrystalline, and the preferred orientation of V₂O₅ is the (001) plane. The morphology of V₂O₅ thin films are porous nature and their particle's shape is three-dimensional. The transmittance and absorbance of thin film were measured from which the optical constants (Energy gap, Refractive index, Absorption coefficient, Extinction coefficient and Optical dielectric constant) were determined.

1. Introduction

Due to their permanent structural flexibility combined with their chemical and physical properties, Vanadium oxides have recently been the subject of much [1, 2]. Because of their permanent structural flexibility associated with their chemical and physical properties. Different oxidation states can be obtained depending on the method of preparation and the type of source material, such as VO₂, V₂O₃ and V₂O₅... [3, 4]. Vanadium pentoxide (V₂O₅) is the most oxidized state, the most stable form of crystallization and most applicable in industry, mainly in Li-ion batteries [5, 6], electrochromic and thermoelectric devices [7, 8], gas sensors [9, 10] and opto- electronic switches [11, 12].

The lamellar structure of V₂O₅ can be distinguished by a series of VO₅ pyramid pairs with roughly square base sharing a ridge. In these pyramids, five oxygen atoms surround the vanadium, one of these atoms is located in the apical position at a shorter distance of about 1.54 Å (this corresponds to a vanadyl bond) [9], and the other atoms are at a distance of about 2 Å. Two pairs of pyramids are linked together by an arete and thus create double zig-zag chains along the axis b. These chains are connected to each other by vertices along an axis and thus form a leaflet. The use of very irregular VO₆ octahedra can also describe the structure, where the sixth oxygen atom is at a greater distance of about 2.79 Å. This link is a type of van der Waals link. The crystal structure of V₂O₅ is an orthorhombic structure where the lattice parameters are a = 11.512 Å, b = 3.564 Å and c = 4.368 Å [8].

Among the methods of preparation of V₂O₅ thin films, we find thermal evaporation, electron beam evaporation [13], magnetron sputtering [14], sol-gel [15], electrochemical deposition [16], pulsed laser ablation [17], and the spray pyrolysis technique [18, 19]. This latter will be the method of preparation used in this work.

The objective of our work is to show the correlation observed between the structural and optical, properties observed in the thin films of V₂O₅ deposited on at different substrate temperatures (350, 400, 450 and 500 °C) using a spray pyrolysis technique.

2. Growth and characterization of V₂O₅

We grow our thin films V₂O₅ by spray pyrolysis method. The precursor used for deposition of films was prepared by dissolving vanadium trichloride (VCl₃) powder in distilled water. They are deposited onto glass substrates, the solution concentration at 0.05 M, the deposition time was 10 min and the substrate temperature varies from 350 °C to 500 °C, The experimental set-up for this last has been described previously [19].

The structural characterizations are performed using X-ray diffraction (XRD) with Cu K α radiation ($\lambda = 1.5406$ Å); the patterns were recorded over the angular range 13–70° (2 θ). Morphology of deposited thin films was observed using FEI Quanta 200 Brand scanning electron microscope. Optical measurements were carried out using the Spectrophotometer JASCO UV/VIS/NIR V570 in the wavelength range (350 – 2500 nm).

* Corresponding author: mrigalasmaa@gmail.com

3. Results and discussion

3.1. Structural properties

Figure 1 shows the XRD patterns for samples grown for different substrate temperatures (350 °C, 400 °C, 450 °C and 500 °C). Analysis by X-ray diffraction showed that all layers are polycrystalline and orthorhombic structure. The preferred orientation of V₂O₅ thin films is the (001) plane at an angle $2\theta = 20.076^\circ$ which indicates the preferred orientation along the crystallographic c axis perpendicular to the substrate. When we have increase substrate temperature, the intensity of the (001) plane peak has been increased. This result may be attributed to the recrystallization process on account of, the increase in the substrate temperature from 400 °C to 500 °C. The obtained results are in agreement with the results reported by Naser and al [20].

Figure 1 also shows that the position of (001) diffraction peak shifts towards higher angle. Indicating that the lattice constant c value of the V₂O₅ thin films decreases with the increase of the substrate temperature (figure 2).

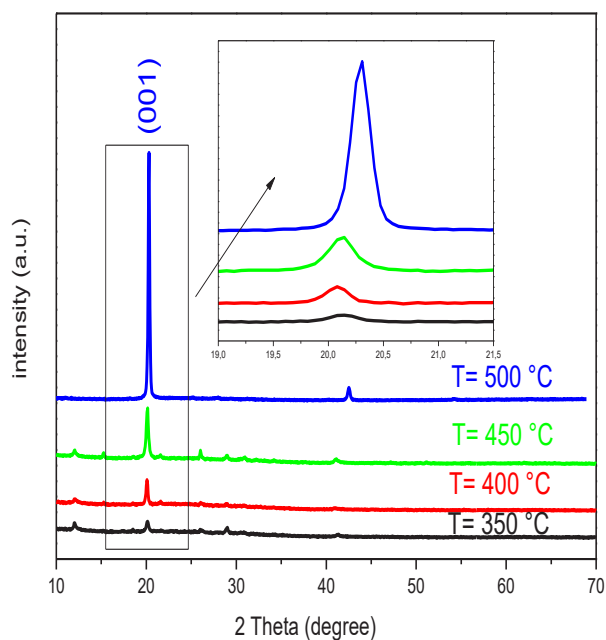


Fig. 1. X-ray diffraction spectra of V₂O₅ samples at different substrate temperatures.

3.2. Morphology

Figure 3 shows the morphology images of V₂O₅ thin films prepared at different substrate temperatures (350, 400, 450 and 500 °C). We can see clearly that there is a change and an evolution of V₂O₅ thin layers shape. Indeed, the layer prepared under 350 °C (Fig 2-a) appears smoother and homogeneous with a small size of grains while the thin films developed under 400, 450 and

500 °C (Fig 3 b-c-d) are inhomogeneous, have a porous nature and their particle's shape is three-dimensional. The same phenomenon was seen on V₂O₅ layers prepared by Liu. & al. [21].

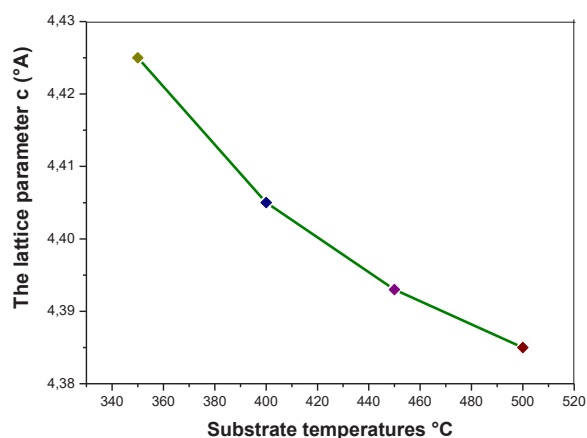


Fig. 2. The lattice parameter c of V₂O₅ samples at different substrate temperatures.

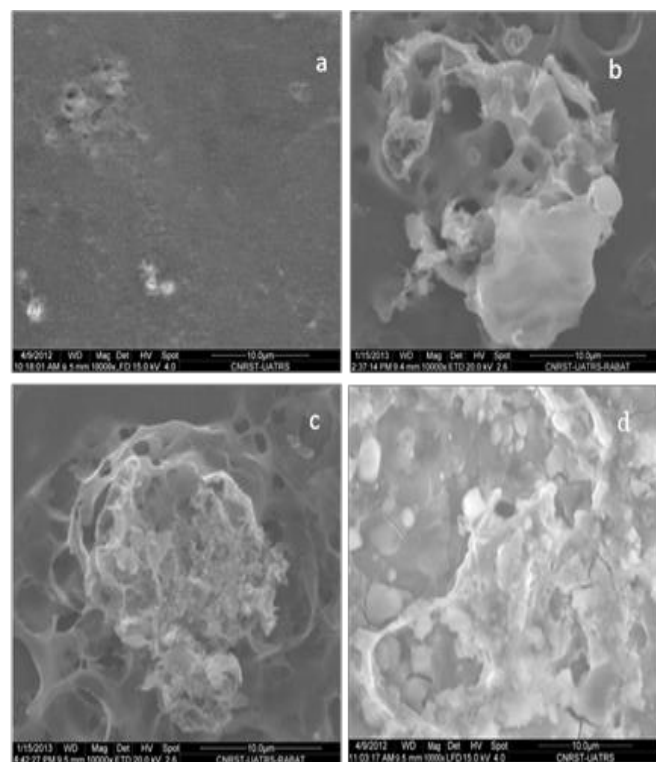


Fig. 3. Surface morphology of V₂O₅ layers at different substrate temperatures.

The layers developed at 500 °C have a high porosity's density. This morphology is very important because it allows the insertion of chemical species (gas, etc...). This helps to consider several applications for those layers especially in the field of electrochromism [22-23].

3.3 Optical properties

Figure 4 shows the optical transmission spectra of V₂O₅ thin layers at the initial state developed in different temperature. All samples exhibit a sharp fundamental absorption edge, and an important transmittance in the visible range, while reflectance is low. In the near IR range the transmittance decreases while the reflectance starts increasing. The same behavior is reported by Ben Ayad et al. [24].

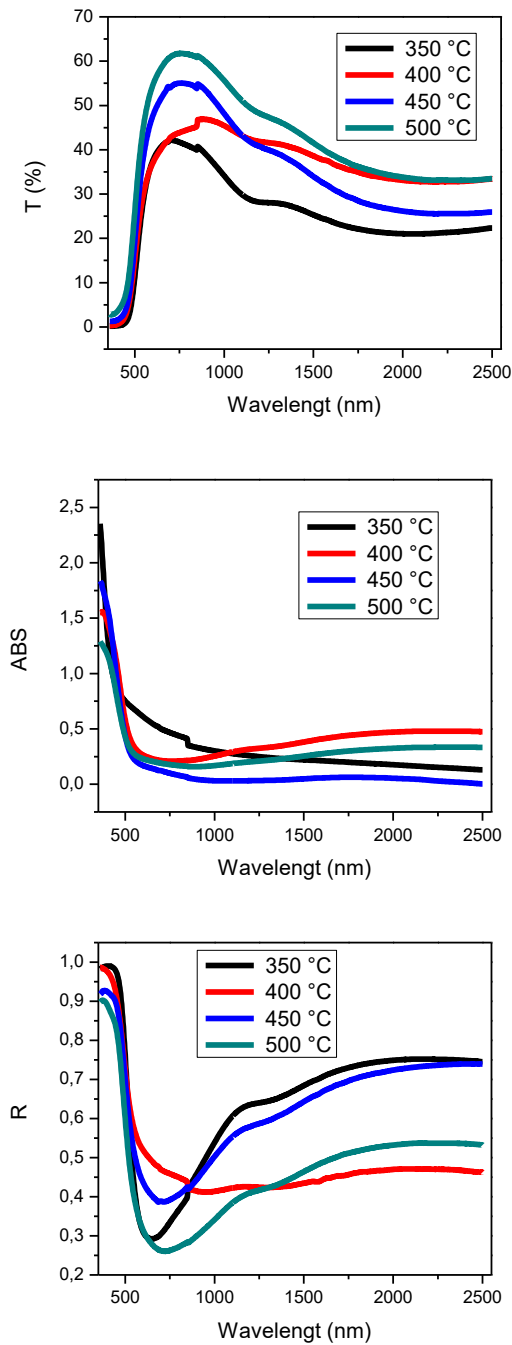


Fig. 4. UV-Vis-NIR Transmission, Absorbance and Reflectance spectra of V₂O₅ thin films with different temperatures.

We can observed that the substrate temperature influence the transmittance value. In fact, when the substrate temperature increases the transmittance value increases. This improvement is mainly related to the crystalline quality of thin films.

The reflectance R of the material with Transmittance (T) and Absorbance (A) is given by the relation:

$$R = 1 - Te^A \quad (1)$$

Transmission values of V₂O₅ with different temperatures (350, 400, 450 and 500 °C) were then used to obtain the values of optical band gap (E_g) by using Tauc [25] and Davis and Mott model [26]. The values of the direct band gaps are 2.46, 2.48, 2.51, 2.52 eV for V₂O₅ thin films elaborated respectively at 350, 400, 450 and 500 °C. These values of direct band gap are comparable to 2.44 eV, already reported by I. Quinzeni et al. for polycrystalline V₂O₅ thin films [27].

The absorption coefficient (α), extinction coefficient (k) and refractive index (n) were determined by the given formulas [28].

$$\alpha = \frac{1}{d} \ln \frac{1}{T} \quad (2)$$

Where α is the absorption coefficient, d and T are the thickness and transmittance of the film respectively.

$$k = \alpha \frac{\lambda}{4\pi} \quad (3)$$

$$n = \frac{1-R}{1+R} + \left(\frac{4R}{(1-R)^2} - k^2 \right)^{1/2} \quad (4)$$

In the figure 5, it is observed that the value of k is decreased and then increased to the insured value with the wavelength, the low 0.6 lower values of the absorption index (k) indicate that these layers are transparent and that the deposited films do not exhibit surface defects. The same behavior is followed by the refractive index n, as shown in the figure 5. The value of the refractive index decreases with increasing wavelength from 500 nm and reaches a saturation value for the high wavelengths.

The real (ε_r) and imaginary (ε_i) parts of the optical dielectric constant can be calculated from the following relations [29] :

$$\epsilon_r = n_2 - k_2 \quad (5)$$

$$\epsilon_i = 2nk \quad (6)$$

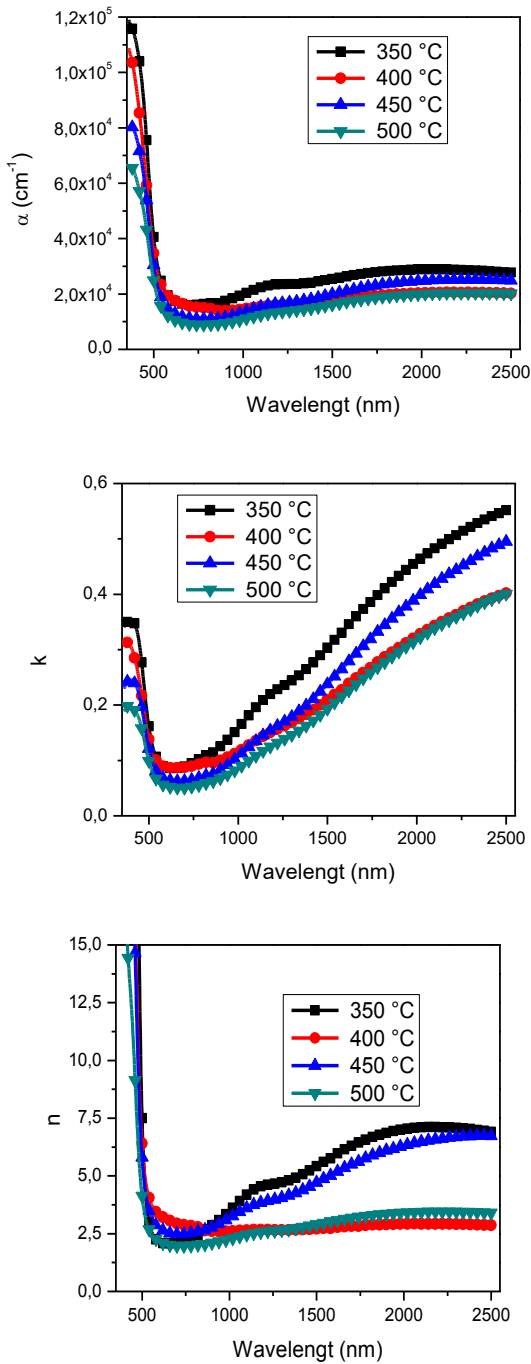


Fig. 5. The absorption coefficient (α), extinction coefficient (k) and refractive index (n) of V_2O_5 thin films with different temperatures.

The optical conductivity is measured using the following formula [30] :

$$\sigma_{opt} = \frac{\alpha \cdot n \cdot c}{4\pi} \quad (7)$$

Where c , α and n is the velocity of light, the absorption coefficient and the refractive index respectively. The figure 6 shows the graph of the real, imaginary parts and the optical dielectric as a function of wavelength in

350-2500 nm range optical conductivity as a function of wavelength ϵ_r and ϵ_i vs wavelength function, also optical conductivity (σ_{opt}) vs wavelength, the values of the real part are greater than those of the imaginary part, these constants show the similar behavior like the k and n .

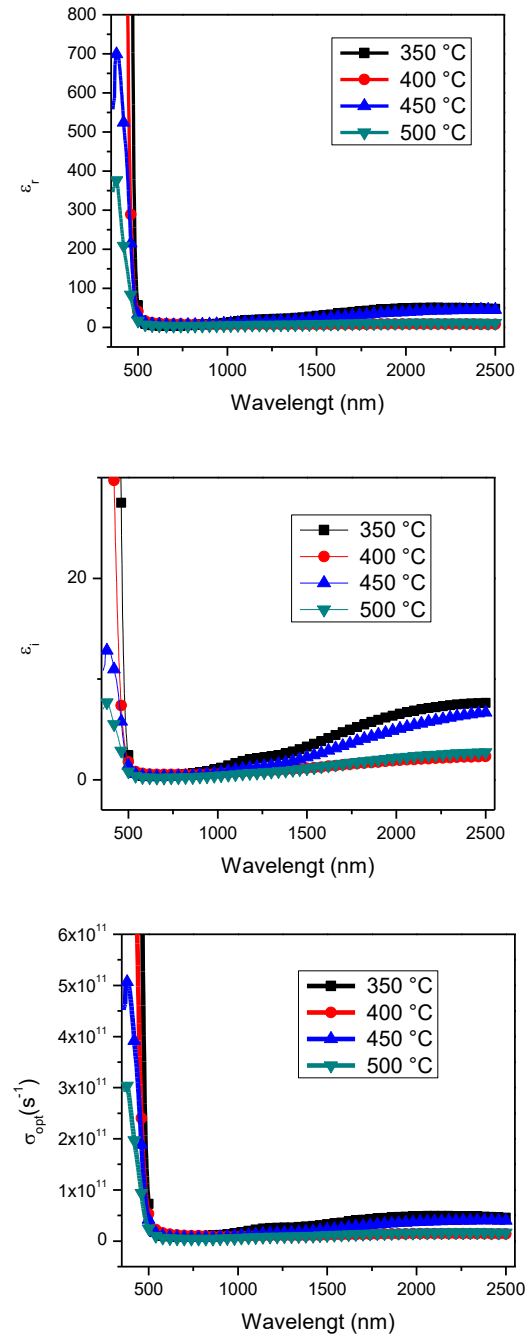


Fig. 6. Plots of variation of the real (ϵ_r) and imaginary (ϵ_i) parts of the optical dielectric and optical conductivity (σ_{opt}) vs wavelength.

The variation of the dielectric constant with the wavelength shows the existence of interactions between photons and electrons in the deposited thin layer [29]. The optical conductivity directly depends on the absorption coefficient and the refractive index of the thin layers and follows the same variation as that of the

absorption coefficient α and the refractive index n when the wavelength increases.

Optical conductivity decreases sharply after 500 nm. This is due to a sharp decrease in the absorption coefficient after this value.

4. Conclusion

To summarize, V_2O_5 films were done by spray pyrolysis method under temperature effect, after characterization, the XRD results shows that all layers are polycrystalline and orthorhombic structure also when the substrate temperature increased the intensity of the pic (001) plane has been increased. The SEM results show that all layers are porous.

The transmission study gives that, substrate temperature improves the transmission of thin films in the visible range, and that the optical gap increases.

In addition, the optical conductivity directly depends on the absorption coefficient and the refractive index of thin layers and follows the same variation as that of the absorption coefficient α and the refractive index n .

In brief, from this study, we can say that V_2O_5 is a promising material for Li-ion batteries and electrochromic devices applications. We are interested to study electrical and electrochemical properties of doped V_2O_5 thin films as a part of future work.

References

1. Y. Cai, G. Fang, J. Zhou, S. Liu, Z. Luo, A. Pan, G. Cao, S. Liang, *Nano Research*, vol. 11, no. 1, pp. 449-463, 2018.
2. I. Valmianski, P. Y. Wang, S. Wang, J. G. Ramirez, S. Guénon, and I. K. Schuller, *Physical Review B*, vol. 98, no. 19, p. 195144, 2018.
3. I. Mjejri, A. Rougier, and M. J. I. c. Gaudon, vol. 56, no. 3, pp. 1734-1741, 2017.
4. H. Liu, D. Wan, A. Ishaq, L. Chen, B. Guo, S. Shi, H. Luo, and Y. Gao, *ACS applied materials & interfaces*, vol. 8, no. 12, pp. 7884-7890, 2016.
5. C. K. Christensen, D. R. Sørensen, J. Hvam, and D. B. Ravnsbæk, *Chemistry of Materials*, vol. 31, no. 2, pp. 512-520, 2018.
6. D. Kong, X. Li, Y. Zhang, X. Hai, B. Wang, X. Qiu, Q. Song, Q. Yanga and L. Zh, *Energy & Environmental Science*, vol. 9, no. 3, pp. 906-911, 2016.
7. I. Mjejri, A. Rougier, and M. Gaudon, *Inorganic chemistry*, vol. 56, no. 3, pp. 1734-1741, 2017.
8. M. Kovendhan, D. Paul, P. Manimuthu, A. Sendilkumar, S.N. Karthick, S. Sambasivam, K. Vijayarangamuthu, H. JeKim, B. Chun Choi, K. Asokan, C. Venkateswaran, R. Mohan, *Current Applied Physics*, vol. 15, no. 5, pp. 622-631, 2015.
9. K. Schneider, M. Lubecka, and A. Czapla, *Sensors and Actuators B: Chemical*, vol. 236, pp. 970-977, 2016.
10. W. Jin, S. Yan, L. An, W. Chen, S. Yang, C. Zhao, Y. Dai, *Sensors and Actuators B: Chemical*, vol. 206, pp. 284-290, 2015.
11. S. B. Zhang, D. W. Zuo, and W. Z. Lu, *Surface Engineering*, vol. 33, no. 4, pp. 292-298, 2017.
12. B.-R. Koo, J.-W. Bae, and H.-J. Ahn, *Ceramics International*, 2019.
13. K. V. Madhuri, B. S. Naidu, O. M. Hussain, M. Eddrief, and C. Julien, *Materials Science and Engineering: B*, vol. 86, no. 2, pp. 165-171, 2001.
14. C. Zhang, Z. Peng, X. Cui, E. Neil, Y. Li, S. Kasap, Q. Yang, *Applied Surface Science*, vol. 433, pp. 1094-1099, 2018.
15. M. R. Loi, E. A. Moura, T. M. Westphal, D.C. Balboni, A. Gündel, W. H. Flores, M. B. Pereira, J. L. Santos, F.L. Santos, A. Pawlicka, C. O. Avellaneda, *Journal of Electroanalytical Chemistry*, 2019.
16. Q. Dong, W. Jiao, L. Lingyan, Z. Hongliang, C. Hongtao, Y. Wei, T. Tian, G. Junhua, Z. Fei, *Journal of Nanoscience and Nanotechnology*, vol. 18, no. 11, pp. 7502-7507, 2018.
17. Y. Deng, A. Pelton, and R. A. Mayanovic, *MRS Advances*, vol. 1, no. 39, pp. 2737-2742, 2016.
18. M. Abbasi, S. M. Rozati, R. Irani, and S. Beke, *Materials Science in Semiconductor Processing*, vol. 29, pp. 132-138, 2015.
19. A. Mrigal, M. Addou, M. El Jouad, M. Hssein, and S. Khannyra, *Sensor letters* Vol. 16, 1-7, 2018.
20. N. M. Abd-Alghafour, Naser. M. Ahmed, Zai. Hassan, Sabah M. Mohammad and M. Bououdina. *AIP Conf. Proc.* 1733, 020026-1-020026-5. 2015.
21. Y. Liu, C. Jia, Z. Wan, X. Weng, J. Xie, L. Deng *Solar Energy Materials & Solar Cells* 132 467-475; 2015.
22. M.B. Sahana, C. Sudakar, C. Thapa, V.M. Naik, G.W. Auner, R. Naik, K.R. Padmanabhan, *Thin Solid Films*, 517 6642-6651 2009.
23. C.E. Patil, N.L. Tarwal, P.S. Shinde, H.P. Deshmukh, P.S. Patil, *J. Phys. D: Appl. Phys.* 42 025404-102009.
24. Z. Ben Ayadi, L. El Mir, K. Djessas, S. Alaya. *Materials Science and Engineering C* 28 613-617 2008.
25. J. Tauc, *Materials Research Bulletin*, vol. 5, no. 8, pp. 721-729, 1970.
26. X. Li, H. Zhu, J. Wei, K. Wang, E. Xu, Z. Li, D. Wu, *Applied Physics A*, vol. 97, no. 2, pp. 341-344, 2009.
27. I. Quinzeni, S. Ferrari, E. Quartarone, and P. Mustarelli, *J. Power Sources*, vol. 196, no. 23, pp. 10228-10233, Dec. 2011.
28. P. Asogwa, *Chalcogenide Letters*, vol. 8, no. 3, pp. 163-170, 2011.
29. A. A. M. Farag and I. S. Yahia, *Optics Communications*, vol. 283, no. 21, pp. 4310-4317, 2010.
30. J. I. Pankove, *Optical processes in semiconductors*. Courier Corporation, 1975.
31. J.-P. Petrakian, *Thin Solid Films*, vol. 38, no. 1, pp. 83-88, 1976.